Epitaxial stabilization of ε-Fe_2O_3 (00l) thin films on $SrTiO_3$ (111)

M. Gich,[1,a)] J. Gazquez,[2] A. Roig,[1,a)] A. Crespi,[1] J. Fontcuberta,[1] J. C. Idrobo,[2,3] S. J. Pennycook,[2,3] M. Varela,[2] V. Skumryev,[4] and M. Varela[5]
[1]*Institut de Ciència de Materials de Barcelona (ICMAB), CSIC, Bellaterra, 08193 Catalunya, Spain*
[2]*Materials Science and Technology Division, Oak Ridge National Laboratory, P.O. Box 2008, Oak Ridge, Tennessee 37831, USA*
[3]*Department of Physics and Astronomy, Vanderbilt University, Nashville, Tennessee 37235, USA*
[4]*Institució Catalana de Recerca i Estudis Avançats (ICREA) and Departament de Física, Universitat Autónoma de Barcelona, Bellaterra, 08193 Catalunya, Spain*
[5]*Departament de Física Aplicada i Óptica, Universitat de Barcelona, Barcelona, 08002 Catalunya, Spain*

(Received 26 December 2009; accepted 20 February 2010; published online 18 March 2010)

Thin films of the metastable and elusive ε-Fe_2O_3 have been epitaxially stabilized on $SrTiO_3$ (111) substrates. The ε-Fe_2O_3 films present a (001) orientation perpendicular to the substrate and three in-plane domains measuring a few nanometers and showing atomically sharp interfaces. We argue that this domain structure, rather than the epitaxial-strain, plays an essential role in stabilizing the ε-Fe_2O_3 by minimizing the energy of (100) surfaces. The ε-Fe_2O_3 films show a large in-plane coercivity ~8 kOe which combined with the magnetoelectric character claimed for this oxide may lead to novel applications in spintronics. © *2010 American Institute of Physics*.
[doi:10.1063/1.3360217]

Progress on magnetoelectric devices, such as tunnel junctions[1] or the magnetoelectric random access memories[2] is fundamentally hampered by the scarcity of suitable materials displaying substantial room-temperature magnetoelectric coupling. Within the oxide realm, antiferromagnetic Cr_2O_3 had been explored[3] although most work is limited to single crystal-based studies. In particular, $GaFeO_3$, a polar ferrimagnet, was among the first materials for which a large linear magnetoelectric effect was reported[4] and has been the object of a renewed interest because it displays magnetically induced second harmonic generation[5] and optical magnetoelectric effects.[6] Only very recently, the growth of $GaFeO_3$ films has also been reported.[7–10]

ε-Fe_2O_3 is a metastable structural intermediate phase of maghemite (γ-Fe_2O_3) and hematite (α-Fe_2O_3) which interestingly, is isostructural to the polar $GaFeO_3$. At room-temperature, it presents a noncentrosymmetric structure (space group $Pna2_1$) where four Fe^{3+} ions are antiferromagnetically coupled along *a*, resulting in a ferrimagnetic ordering.[11,12] ε-Fe_2O_3 has a large room-temperature coercivity of 20 kOe[13] and enlarges the family of magnetoelectric oxides since it presents a coupling of its magnetic and dielectric properties.[14] It has been recently established that the large magnetic anisotropy in ε-Fe_2O_3 is provoked by distortions of the Fe^{3+} coordination polyhedra which are responsible for a substantial spin-orbit coupling.[15] Thus, *a priori*, ε-Fe_2O_3 should display superior properties than other known room-temperature magnetoelectric oxides owing it to (i) its ferrimagnetic character and in contrast to the antiferromagnetism displayed by Cr_2O_3, and to (ii) its Curie temperature, which is much higher (510 K) than that of $GaFeO_3$ (200 K). Moreover, the fact that this is a single-metal, single-valent oxide offers an advantage over other multimetallic and/or mixed valence systems in which a control of site occupancies is required for optimum response.

So far, ε-Fe_2O_3 has only been grown as nanoparticles in confined nanoreactors by sol-gel based methods[12,13,16] or as nanowires.[17,18] Therefore, in spite of its obvious interest, implementation of ε-Fe_2O_3 in practical devices was challenged by the absence of thin films.

In the present letter, we show that using appropriate substrates, epitaxial stabilization of ε-Fe_2O_3 thin films has been achieved. We claim that twinning and interface energies, rather than the common substrate-induced epitaxial strain, play crucial roles on the stabilization of this phase.

Iron oxide films of about 100 nm thickness were grown on several substrates as follows: Si (100), MgO (100), yttria-stabilized zirconia (111), and STO (111). A Kr excimer laser (248 nm wavelength, 34 ns pulse duration) was used at a 5 Hz repetition rate, focused at ~1.5 J/cm^2 on a α-Fe_2O_3 target placed at a distance of 5 cm. The target was prepared by sintering α-Fe_2O_3 powders (Aldrich 99.9% purity). The growth conditions were chosen following the conditions that yielded high density 1D nanowire growth in Ref. 17. The substrate temperature was 800 °C. The oxygen pressure was maintained at 9.86×10^{-5} atm during the sample growth and increased to 1 atm once the substrate temperature reached 500 °C on cooling. The crystal structure of the films was analyzed by x-ray diffraction (XRD) using Cu $K\alpha$ radiation in a Bruker-AXS D8 Advance diffractometer and by transmission electron microscopy (TEM) and scanning TEM (STEM). Conventional TEM and selected-area electron diffraction (SAED) were carried out on a FEI CM-200 transmission electron microscope operating at 200 kV. Atomic resolution Z-contrast images were taken at 300 kV in a FEI Titan 80–300 S scanning transmission electron microscope and in two dedicated STEMs VG HB603U at 300 kV and NION UltraSTEM at 100 kV. Specimens for TEM and STEM were prepared by ion milling to electron transparency (~100 nm). A Quantum Design superconducting quantum interference device magnetometer was used for the magnetic characterization.

[a)]Authors to whom correspondence should be addressed. Electronic addresses: marti.gich@gmail.com and roig@icmab.es.

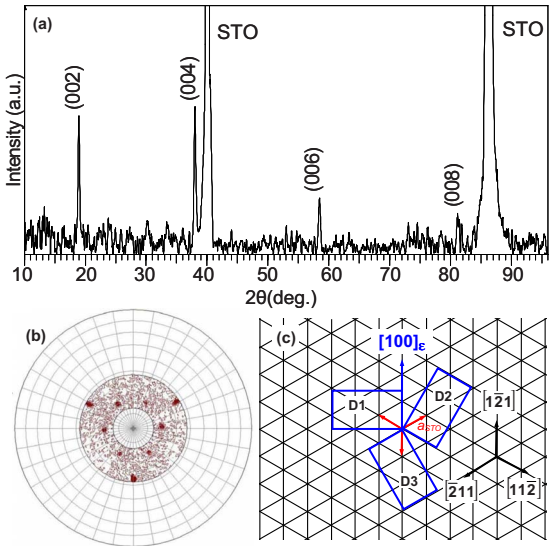

FIG. 1. (Color online) (a) XRD θ-2θ scan of ε-Fe_2O_3 film grown on (111) STO. (b) Pole figures of the $\{013\}_\varepsilon$ and $\{110\}_{STO}$ poles. The divisions of the azimuth and polar coordinates are of 10°. (c) Schematic drawing of the domain structure. The short arrows indicate the unit cell of STO, and the long arrows refer to the in-plane directions on (111) STO.

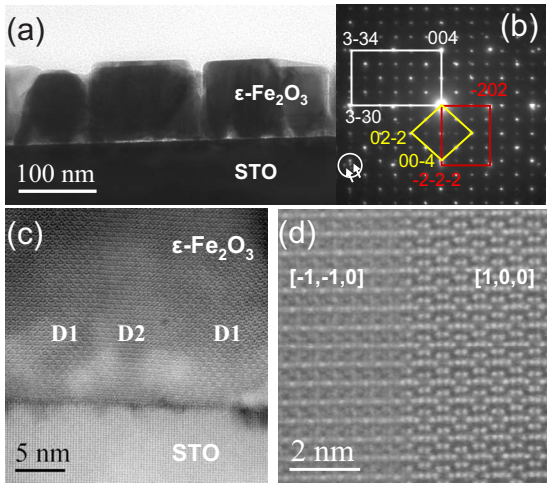

FIG. 2. (Color online) (a) Cross-sectional TEM image of the sample grown on (111) STO. (b) SAED pattern indexed considering the superposition of the diffraction patterns along the zone axes [100] and $[\bar{1}\bar{1}0]$ of ε-Fe_2O_3 and $[1\bar{2}1]$ of STO, diamond, oblong, and square parallelograms, respectively. (c) Z-contrast STEM image of the ε-Fe_2O_3/STO interface. (d) Atomic resolution Z-contrast image of the interface between D1 and D2 domains.

We performed XRD analysis of the films grown on the different substrates. Textured growth has only been observed on YSZ(111), showing γ-Fe_2O_3 $(0kl)$ reflections (not shown), and on STO(111) where ε-Fe_2O_3 has been stabilized. The θ-2θ XRD scan of the latter [Fig. 1(a)] only shows reflections corresponding to ε-Fe_2O_3. The peaks observed at 2θ=18.94°, 38.17°, 58.68°, and 81.42° can be, respectively, ascribed to the (002), (004), (006), and (008) reflections, indicating an out-of plane $\{001\}_\varepsilon \| \{111\}_{STO}$ orientation relationship of the ε-Fe_2O_3 film. We find that the c cell parameter extracted by the Nelson Riley extrapolation method[19] to θ=90° is 9.467(5) Å which is essentially the same reported for nanoparticles at room temperature,[20] indicating that the film is strain-relaxed. In order to get an average picture of the in-plane texture of the ε-Fe_2O_3 film, two pole figures were recorded for 2θ=30.06° and 2θ=32.4° which correspond to the Bragg condition of the (013) and (110) reflections of ε-Fe_2O_3 and STO, respectively [see Fig. 1(b)]. The pole figure exhibits the three equivalent {110} STO poles at a tilt angle $\psi \sim 35.3°$, providing the in-plane orientation of the substrate for reference. Decreasing the tilt to the substrate normal one finds six poles rotated at 60° one to each other in azimuth (ϕ) at $\psi \sim 20°$ which correspond to the {013} planes of the (00l)-oriented ε-Fe_2O_3. In order to understand the in-plane orientation which is derived from this pole arrangement, one must consider that the projections of the $\{013\}_\varepsilon$ and $\{110\}_{STO}$ poles on the $(001)_\varepsilon$ and $(111)_{STO}$ planes are parallel to $[010]_\varepsilon$ and $[11\bar{2}]_{STO}$ directions, respectively. The angle between the $[11\bar{2}]_{STO}$ and $[10\bar{1}]_{STO}$, contained in the $(111)_{STO}$ plane is 30°, and since the $\{013\}_\varepsilon$ pole only consists of the (013) and $(0\bar{1}3)$ planes, with poles 180° apart in ϕ, it can be deduced from the pole figure that the ε-Fe_2O_3 film presents three in-plane domains rotated 120° to each other, reflecting the threefold symmetry of the STO(111) planes. Thus, the in-plane orientation of the first domain, D1, is $[010]_\varepsilon \| [10\bar{1}]_{STO}$ (i.e., $[100]_\varepsilon \| [1\bar{2}1]_{STO}$) and domains D2 and D3 have $[100]_\varepsilon \| [11\bar{2}]_{STO}$ and $[100]_\varepsilon \| [\bar{2}11]_{STO}$ orientations. This in-plane domain structure is represented in Fig. 1(c).

Figure 2(a) shows a cross-sectional TEM image of the ε-Fe_2O_3 layer grown on STO (111) substrate. The film presents a uniform thickness (of about 110 nm) and a uniform grain structure. The coalesced grains have a rectangular shape and a flat surface. Some grains also present irregularities at the interface in the form of voids. Nevertheless, the corresponding SAED pattern, Fig. 2(b), shows an epitaxial growth of the ε-Fe_2O_3 film on STO, in good agreement with the XRD observations. The diffraction spots of the SAED pattern can be indexed by considering the superposition of the diffraction patterns obtained along the zone axes [100] and $[\bar{1}\bar{1}0]$ of ε-Fe_2O_3 and $[1\bar{2}1]$ of STO indicating the presence of the domains D1 and D2 with the c-axis normal to the substrate surface. The SAED pattern also confirms the relaxation of the film, showing the splitting of the film and substrate diffraction spots [see arrows in Fig. 2(b)].

Figure 2(c) shows a Z-contrast STEM image of the ε-Fe_2O_3/STO interface along the $[1\bar{2}1]$ STO zone axis. The ε-Fe_2O_3/STO interface is sharp and presents periodic strain contrast due to misfit dislocations. Figure 2(c) also shows domains D1 and D2 which are ~5 nm across, extending the full thickness of the film. Figure 2(d), a higher resolution Z-contrast image, reveals an atomically sharp interface between the two ε-Fe_2O_3 domains.

The alternating Ti^{4+} and SrO_3^{4-} layers with threefold symmetry in the STO (111) substrate act as nucleation sites for ε-Fe_2O_3 basal planes but with a relatively large lattice mismatch;[20] $(\sqrt{6}a_{STO}-2a_\varepsilon)/2a_\varepsilon \sim -6.2\%$ and $(3\sqrt{2}a_{STO}-2b_\varepsilon)/2b_\varepsilon \sim -5.7\%$ for $[100]_\varepsilon \| [1\bar{2}1]_{STO}$ and $[010]_\varepsilon \| [30\bar{3}]_{STO}$, respectively. The large lattice mismatch between the substrate and the film could explain why only very small domains (of ~ few nanometers) have nucleated.

Even though previous studies of $GaFeO_3$ grown on STO(111) reported the same (001) texture[10] as observed in this study for ε-Fe_2O_3, the conditions of ε-Fe_2O_3 stabilization are more critical than for $GaFeO_3$. For instance, while $GaFeO_3$ (110) grows epitaxially on MgO (100),[9] Fe_2O_3 de-

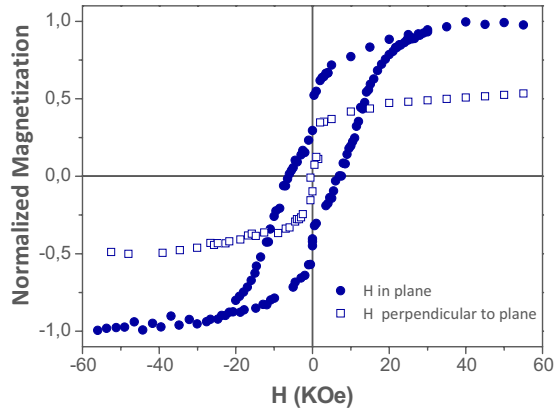

FIG. 3. (Color online) Hysteresis loops at 300 K measured with the magnetic field applied parallel (full circles) and perpendicular (empty squares) to the substrate. Data has been corrected for the diamagnetic contribution of the substrate.

posited at essentially the same conditions does not. This may be related to the fact that ε-Fe_2O_3 nanoparticles present a marked tendency to grow anisotropically along the [100] direction,[21,22] likely because the energy of the (100) surfaces is particularly high. Indeed, any $[100]_\varepsilon$ out of plane texture would be clearly unfavorable. However, the domain structure that we have observed (i. e. domains ~5 nm at 120° to each other) could contribute to reduce the energy of the ε-Fe_2O_3 (100) surfaces through the domain boundaries. It is interesting to note that the growth of ε-Fe_2O_3 with $[001]_\varepsilon$ in-plane is not observed, even with the c lattice parameter of ε-Fe_2O_3 (c_ε=9.468 Å) presenting a low mismatch along $[1\bar{2}1]_{STO}$ [i.e., $(\sqrt{6}a_{STO}-c_\varepsilon)/c_\varepsilon \sim 1\%$]. This means that either $[100]_\varepsilon$ is out of plane implying the existence of high energy (100) surfaces, or both a and c in-plane with $[001]_\varepsilon \| [1\bar{2}1]_{STO}$ and $[100]_\varepsilon \| [30\bar{3}]_{STO}$ which has a high lattice mismatch $[(\sqrt{2}a_{STO}-a_\varepsilon)/a_\varepsilon \sim 8.5\%]$.

Hysteresis loops M(H) were measured, at room temperature, with the magnetic field applied parallel and perpendicular to the film plane (Fig. 3). The shape of the loop measured with in-plane field is consistent with the domain structure described above and with the data reported for magnetic-field oriented nanorods.[20] In the films, the crystallographic a-axis, which corresponds to the easy magnetization axis, forms a network of domains oriented at 120° from each other. Therefore, assuming that the magnetization process takes place via coherent rotation of the magnetization vector, the resulting H_C should be intermediate between the value measured in a in-plane field applied along the easy a-axis and perpendicular to it and accordingly, the shape of the loop will be less rectangular than the loop measured along a. Indeed, this is what we observed experimentally (H_C ~8 kOe). Finally, one notices a magnetization step in the low-field region of the return branch of the M(H) curve. This shoulder could be attributed to the presence of a small fraction of superparamagnetic γ-Fe_2O_3.[23] Such claim is further confirmed by the shape of the magnetization loop measured with the field perpendicular to the film plane, and to the easy axis (Fig. 3).

In conclusion, we have shown that it is possible to prepare epitaxial thin films of the metastable ε-Fe_2O_3 with good quality on STO (111) substrates using pulsed laser deposition. The coercivity of the films measured from hysteresis loops is ~8 kOe, which is well below the ~20 kOe measured in nanoparticles, but consistent with the domain structure observed in this study. The ε-Fe_2O_3 films present a (001) orientation perpendicular to the substrate and three types of in-plane domains rotated 120° to each other with $[100]_\varepsilon \| [1\bar{2}1]_{STO}$. The domains show atomically sharp interfaces, with sizes between 5–10 nm. We argue that this domain structure can play an essential role in the film stabilization by minimizing the energy of the ε-Fe_2O_3 (100) surfaces. The high coercivity displayed by the ε-Fe_2O_3 films and the magnetoelectric character of ε-Fe_2O_3 can be appealing for its application in spintronics and its future integration into devices.

This research was partially supported by the Ministerio de Ciencia e Innovacion (Grant Nos. MAT2009-08024 and CSD2007-00041), the Office of Basic Energy Sciences, Division of Materials Sciences and Engineering, U.S. Department of Energy (S.J.P and M.V.), and the SHaRE User Facility (J.G. and J.C.I.).

[1] M. Gajek, M. Bibes, S. Fusil, K. Bouzehouane, J. Fontcuberta, A. Barthelemy, and A. Fert, Nature Mater. **6**, 296 (2007).
[2] X. Chen, A. Hochstrat, P. Borisov, and W. Kleemann, Appl. Phys. Lett. **89**, 202508 (2006).
[3] P. Borisov, A. Hochstrat, X. Chen, W. Kleemann, and Ch. Binek, Phys. Rev. Lett. **94**, 117203 (2005).
[4] G. T. Rado, Phys. Rev. Lett. **13**, 335 (1964).
[5] Y. Ogawa, Y. Kaneko, J. P. He, X. Z. Yu, T. Arima, and Y. Tokura, Phys. Rev. Lett. **92**, 047401 (2004).
[6] N. Kida, Y. Kaneko, J. P. He, M. Matsubara, H. Sato, T. Arima, H. Akoh, and Y. Tokura, Phys. Rev. Lett. **96**, 167202 (2006).
[7] D. C. Kundaliya, S. B. Ogala, S. Dhar, K. F. McDonald, E. Knoesel, T. Osedach, S. E. Lofland, S. R. Shinde, and T. Venkatesan, J. Magn. Magn. Mater. **299**, 307 (2006).
[8] M. Trassin, N. Viart, G. Versini, J.-L. Loison, J.-P. Vola, G. Schmerber, O. Crégut, S. Barre, G. Pourroy, J. H. Lee, W. Jo, and C. Mény, Appl. Phys. Lett. **91**, 202504 (2007).
[9] Z. H. Sun, S. Dai, Y. L. Zhou, L. Z. Cao, and Z. H. Chen, Thin Solid Films **516**, 7433 (2008).
[10] Z. H. Sun, Y. L. Zhou, S. Y. Dai, L. Z. Cao, and Z. H. Chen, Appl. Phys. A: Mater. Sci. Process. **91**, 97 (2008).
[11] E. Tronc, C. Chanéac, and J. P. Jolivet, J. Solid State Chem. **139**, 93 (1998).
[12] M. Gich, C. Frontera, A. Roig, E. Taboada, E. Molins, H. R. Rechenberg, J. D. Ardisson, W. A. A. Macedo, C. Ritter, V. Hardy, J. Sort, V. Skumryev, and J. Nogués, Chem. Mater. **18**, 3889 (2006).
[13] J. Jin, S. Ohkoshi, and K. Hashimoto, Adv. Mater. (Weinheim, Ger.) **16**, 48 (2004).
[14] M. Gich, C. Frontera, A. Roig, J. Fontcuberta, E. Molins, N. Bellido, C. Simon, and C. Fleta, Nanotechnology **17**, 687 (2006).
[15] Y.-C. Tseng, N. M. Souza-Neto, D. Haskel, M. Gich, C. Frontera, A. Roig, M. van Veenendaal, and J. Nogués, Phys. Rev. B **79**, 094404 (2009).
[16] M. Gich, A. Roig, E. Taboada, E. Molins, C. Bonafos, and E. Snoeck, Faraday Discuss. **136**, 345 (2007).
[17] J. R. Morber, Y. Ding, M. Haluska, Y. Li, J. P. Liu, Z. L. Wang, and R. L. Snyder, J. Phys. Chem. B **110**, 21672 (2006).
[18] Y. Ding, J. R. Morber, R. L. Snyder, and Z. L. Wang, Adv. Funct. Mater. **17**, 1172 (2007).
[19] J. B. Nelson and D. B. Riley, Proc. Phys. Soc. London **57**, 160 (1945).
[20] M. Gich, A. Roig, C. Frontera, E. Molins, J. Sort, M. Popovici, G. Chouteau, D. Martín y Marero, and J. Nogués, J. Appl. Phys. **98**, 044307 (2005) (room temperature lattice parameters used for epsilon a_ε =5.098 Å, b_ε=8.785 Å, c_ε=9.468 Å. Value used for STO a_{STO} =3.905 Å).
[21] S. Sakurai, J.-I. Shimoyama, K. Hashimoto, and S. Ohkoshi, Chem. Phys. Lett. **458**, 333 (2008).
[22] Y. Kusano, T. Fujii, J. Takada, M. Fukuhara, A. Doi, Y. Ikeda, and M. Takano, Chem. Mater. **20**, 151 (2008).
[23] E. Taboada, M. Gich, and A. Roig, ACS Nano **3**, 3377 (2009).